Deposition of Bismuth Chalcogenide Thin Films Using Novel Single-Source Precursors by Metal-Organic Chemical Vapor Deposition

John Waters, David Crouch, James Raftery, and Paul O'Brien*

The Manchester Materials Science Centre and Department of Chemistry, The University of Manchester, Oxford Road, Manchester, M13 9PL, U.K.

Received December 8, 2003. Revised Manuscript Received March 5, 2004

The metal-organic compounds, $Bi[(EPR_2)_2N]_3$ (E = S, Se; R = Ph, ^{i}Pr), have been synthesized and used as single-source precursors for the deposition of bismuth chalcogenide thin films via low-pressure and aerosol-assisted metal-organic chemical vapor deposition. Crystalline thin films of rhombohedral Bi_2Se_3 (using $Bi[(SeP^iPr_2)_2N]_3$), hexagonal BiSe (using $Bi[(SePPh_2)_2N]_3$), and orthorhombic Bi_2S_3 (using $Bi[(SPR_2)_2N]_3$) have been deposited on glass substrates. Films have been characterized by X-ray powder diffraction, scanning electron microscopy, and energy-dispersive analysis of X-rays.

1. Introduction

Bismuth selenide is a V/VI semiconductor with a band gap of ca. 0.3 eV,[1,2] which is suitable for applications in optical and photosensitive devices, in photoelectrochemical (PEC) cells, in solar-selective decorative coatings, and in the fabrication of an ideal Hall effect magnetometer.[3−5] Films of Bi_2Se_3 have previously been prepared by chemical bath deposition (CBD),[6−8] electrodeposition,[9] molecular jet,[10] successive ionic layer adsorption and reaction (SILAR)[11,12] methods, and melting together high-purity bismuth and selenium under vacuum.[13]

Bismuth sulfide has a direct band gap of 1.3 eV[14] and has been the subject of significant research in recent years due to its potential for use in photodiode arrays,[15] thermoelectric coolers,[16] and photoelectrochemical cells.[17] Variano et al. have reported the preparation of disk-like particles of Bi_2S_3, prepared in microemulsions.[18] Nanorods of orthorhombic Bi_2S_3 have also been prepared by microwave irradiation of solutions of bismuth nitrate and thiourea.[19] Boudjouk et al. have employed benzylthiolato bismuth compounds as single-source precursors for the preparation of Bi_2S_3 via pyrolysis.[20] Monterio et al. have reported the synthesis of nano- and micro-sized particles of Bi_2S_3.[21] Materials were prepared by thermolysis of precursors of the type $Bi(S_2CNRR')_2$, in hot (ca. 150 °C) tri-*n*-octylphosphine oxide (TOPO) and under reflux conditions in 2-ethoxyethanol, ethyleneglycol, 4-ethylpyridine, and *p*-xylene. These workers also studied the deposition of thin films of Bi_2S_3 from bismuth dithiocarbamates, $Bi(S_2CNRR')_3$ (R = ethyl, R′ = ethyl and R = methyl, R′ = hexyl) at T_{subs} = 400−450 °C by LP-MOCVD (low-pressure metal-organic chemical vapor deposition).[22] The resulting films were found to be composed of nanofibers of orthorhombic Bi_2S_3, with direct band gaps of 1.29 eV. In further work by Tiekink et al.,[23] bismuth trisxanthate and dithiocarbamate precursors are employed for the synthesis of Bi_2S_3 nanoparticulates by solvent thermalysis and for the deposition of thin films via CVD. Films of Bi_2S_3 have also been deposited by chemical bath and electrospray techniques with a variety of sulfur sources such as thiourea, thioacetamide, and thiosulfate.[24−29]

* Corresponding author. Professor Paul O'Brien, Department of Chemistry, University of Manchester, Oxford Road, Manchester, M13 9PL, U.K. Tel: +44 (0)161 275 4652. Fax: +44 (0)161-275-4616. E-mail: paul.obrien@man.ac.uk.

(1) Mishra, S. K.; Satpathy, S.; Jepsen O. *J. Phys.: Condens. Matter* **1997**, *9*, 461.
(2) Black, J.; Conwell, E. M.; Seigle, L.; Spencer, C. W. *J. Phys. Chem. Solids* **1957**, *2*, 240.
(3) Sakai, N.; Kajiwara, T.; Takemura, K.; Minomura, S.; Fuji, Y. *Solid State Commun.* **1981**, *40*, 1045.
(4) Yesugade, N. S.; Lokhande, C. D.; Bhosale, C. H. *Thin Solid Films* **1995**, *263*, 145.
(5) Woolam, J. A.; Beale, H. A.; Spain, I. L. *Rev. Sci. Instrum.* **1973**, *44*, 434.
(6) Pramanik, P.; Bhattacharya, R. N.; Mondal, A. *J. Electrochem. Soc.* **1980**, *127*, 1857.
(7) Bhattcharya, R. N.; Pramanik, P. *J. Electrochem. Soc.* **1982**, *129*, 332.
(8) Garcia, M.; Nair, M. T. S.; Nair, P. K.; Zingaro, R. A. *Semicond. Sci. Technol.* **1997**, *12*, 645.
(9) Torane, A. P.; Lokhande, C. D.; Patil, P. S.; Bhosale, C. H. *Mater. Chem. Phys.* **1998**, *55*, 51.
(10) Boyer, A.; Charles, E. *Vide* **1991**, *46*, 99.
(11) Sankapal, B. R.; Mane, R. S.; Lokhande, C. D. *Mater. Chem. Phys.* **2002**, *63*, 230.
(12) Nataraj, D.; Senthil, K.; Narayandass, S. A. K.; Mangalaraj, D. *Cryst. Res. Technol.* **1999**, *34*, 867.
(13) Sankapal, B. R.; Lokhande, C. D. *Mater. Chem. Phys.* **2002**, *73*, 151.
(14) Nomura, R.; Kanaya, K.; Matsuda, H. *Bull. Chem. Soc. Jpn.* **1989**, *62*, 939.
(15) Pawar, S. H.; Bhosale, P. N.; Uplane, M. D.; Tamhankar, S. *Thin Solid Films* **1983**, *110*, 165.
(16) Killedar, V. V.; Lokhande, C. D.; Bhosale, C. H. *Thin Solid Films* **1996**, *286*, 14.
(17) Mane, R. S.; Sankapal, B. R.; Lokhande, C. D. *Chem. Phys.* **1999**, *60*, 196.
(18) Variano, B. F.; Hwang, D. M.; Sandroff, C. J.; Witlzius, P.; Jing, T. W.; Ong, N. P. *J. Phys. Chem.* **1987**, *91*, 6455.
(19) Liao, X.-H.; Wang, H.; Zhu, J.-J.; Chen, H.-Y. *Mater. Res. Bull.* **2001**, *36*, 2339.
(20) Boudjouk, P.; Remington Jr., M. P.; Grier, D. G.; Jarabek, B. R.; McCarthy, G. J. *Inorg. Chem.* **1998**, *37*, 3538.
(21) Monteiro, O. C.; Nogueira, H. I. S.; Trindade, T.; Motevalli, M. *Chem. Mater.* **2001**, *13*, 2103.
(22) Monteiro, O. C.; Trindade, T.; Park, J.-H.; O'Brien, P. *Chem. Vap. Deposition* **2000**, *6*, 230.
(23) Koh, Y. W.; Lai, C. S.; Du, A. Y.; Tiekink, E.; Loh, K. P. *Chem. Mater.* **2003**, *15*, 4544.
(24) Wang, S. Y.; Du, Y. W. *J. Cryst. Growth* **2002**, *236*, 627.

10.1021/cm035287o CCC: $27.50
Published on Web 07/23/2004

Recently, we have reported the growth of II/VI thin films from $M[(SePPh_2)_2N]_2$ (M = Cd(II), Zn(II)) by LP-MOCVD.[30] These precursors have been found to be suitable single-source precursors for the deposition of II/VI materials. Our further studies on precursors based on the $NH(EPR_2)_2$ ligand have now been extended to include dichalcogenoimidodiphoshanto bismuth. In this paper, we report the growth of bismuth chalcogenide films from $Bi[(EPR_2)_2N]_3$ (E = S, Se; R = Ph, ^{i}Pr) on glass substrates by LP and AACVD (AA = aerosol-assisted).

2. Experimental Section

Unless otherwise stated, all reactions were performed under an atmosphere of dry nitrogen using standard Schlenk techniques. All glassware was flame-dried under vacuum prior to use. All solvents and reagents were purchased from Sigma-Aldrich Chemical Co. and used as received. NMR studies (^{1}H and ^{31}P) were carried out using a Bruker AC300 FTNMR spectrometer. Mass spectra were recorded on a Kratos concept 1S instrument. Infrared spectra were recorded on a Specac single reflectance ATR instrument. Elemental analysis was conducted at the Microanalytical department at the University of Manchester.

2.1. Precursor Synthesis. Precursors were synthesized according to literature methods[31] as reported previously.[32] The dichalcogenoimidodiphoshanto ligands were synthesized by the reaction of hexamethyl disilazane with the relevant chlorophosphine, before refluxing with the desired chalcogen. The sodium salts of the ligands were generated by reaction of the ligand with sodium methoxide. The precursors were prepared by the reaction of the sodium salts with bismuth(III) nitrate pentahydrate.

2.2. Single-Crystal X-ray Diffraction Study. Crystal data for $Bi[(SP^iPr_2)_2N]_3$: $C_{36}H_{70}BiN_3P_6S_6$, M = 1132.11, monoclinic, space group *Cc*, a = 23.54(5) Å, b = 13.326(5) Å, c = 19.281(5) Å, α = 90°, β = 117.100(7)°, γ = 90°, V = 5342(3) Å^3, Z = 4, D_c = 1.408 mg m^{-3}, μ(Mo Kα) = 3.742 mm^{-1}, F(000) = 2304, T = 100(2) K, monochromated Mo Kα radiation, λ = 0.71073 Å; the total number of measured and observed independent reflections are 22774 and 6357 (R_{int} = 0.1092). R1 = 0.0648 and wR2 = 0.1151. One of the *iso*propyl groups bonded to P2 showed evidence of disorder. An alternative conformation was defined corresponding to an approximately 180° rotation about P2−C10 and the model refined with the occupancy of the conformations as varibles but the sum constrained to be equal to 1. The structures were solved by direct methods and refined by full-matrix least-squares on F^2.[33] All calculations were carried out using the SHELXTL package.[34] All non-hydrogen atoms were refined with anisotropic atomic displacement parameters. Hydrogen atoms were placed in calculated positions, assigned isotropic thermal parameters, and allowed to ride on their parent carbon atoms. Crystallographic data and selected interatomic distances and angles are summarized in Tables 1 and 2, respectively.

Table 1. Crystallographic Data and Structure Refinement Parameters for $Bi[(SP^iPr_2)_2N]_3$

formula	$C_{36}H_{70}BiN_3P_6S_6$
fw	1132.11
λ (Å)	0.71073
crystal system	monoclinic
a (Å)	23.354(5)
b (Å)	13.326(5)
c (Å)	19.281(5)
α (deg)	90
β (deg)	117.100(7)
γ (deg)	90
V (Å^3)	5342(3)
Z	4
space group	*Cc*
d_{calcd} (mg/m^3)	1.408
μ (mm^{-1})	3.742
no. of reflections collected	22774
no. of unique reflections	6357
R indices [$I > 2\sigma(I)$]	R1 = 0.0648 wR2 = 0.1151
R indices (all data)	R1 = 0.0863 wR2 = 0.1222
max. peak and hole	0.8960−0.7060

Table 2. Selected Bond Lengths (Å) and Angles (deg) for $Bi[(SP^iPr_2)_2N]_3$

Bi(1)−S(1)	2.831(2)	S(1)−Bi(1)−S(6)	165.99(5)
Bi(1)−S(2)	2.775(2)	S(1)−Bi(1)−S(2)	88.33(6)
Bi(1)−S(5)	2.843(2)	S(1)−Bi(1)−S(5)	79.74(6)
N(1)−P(1)	1.594(6)	S(1)−Bi(1)−S(3)	112.17(8)
N(1)−P(2)	1.591(6)	S(1)−Bi(1)−S(4)	79.39(9)
N(3)−P(5)	1.584(4)	S(2)−Bi(1)−S(3)	79.39(9)
P(1)−S(1)	2.038(3)	S(2)−Bi(1)−S(5)	109.21(9)
P(2)−S(2)	2.034(3)	S(2)−Bi(1)−S(4)	157.97(14)
P(5)−S(5)	2.027(3)	S(3)−Bi(1)−S(4)	88.33(9)
		N−P−S	118.0(3)−120.3(3)
		P−S−Bi	111.17(9)−117.41(10)

The CCDC reference number is 225800.

2.3. Preparation of Thin Films by LP-MOCVD. In these studies a cold wall, horizontal reactor was used. The glass substrates were heated by a tungsten halogen lamp. A Carbolite tube furnace was used to deliver the precursor (∼200 mg) under a dynamic vacuum at ≈10^{-2} Torr. Experiments were conducted for growth periods of 1 h.

2.4. Preparation of Thin Films by AACVD. In these experiments, the precursor (∼200 mg) was dissolved in THF (30 mL). Glass substrates were heated by a Carbolite tube furnace. Aerosol droplets of the precursor solution were generated by the piezoelectric modulator of an ultrasonic humidifier. A Platon flow gauge was used to control the flow of the argon carrier gas at constant flow rates of 140 and 200 sccm, enabling controlled delivery of aerosol droplets into the deposition chamber.

2.5. Characterization of Thin Films. X-ray powder diffraction studies were performed using a Bruker AXS D8 diffractometer using monochromated Cu Kα radiation, with scans over 2θ values of 5°−90° in steps of 0.01 or 0.02°. SEM was carried out on a Philips 525 or a Philips XL30 FEG instrument and EDAX was preformed using a DX4. Films were carbon-coated using an Edward's E306A coating system. TGA measurements were carried out on a Seiko SSC/S200 model under nitrogen, from 25 to 600 °C, with a heating rate of 10 °C/min. Pyrolysis was carried out using a Carbolite tube furnace, heating a precursor (ca. 0.3 g) to 600 °C for 1 h, under argon at atmospheric pressure. Grain size distributions for films were performed using an image analysis program (CGS2).[35] Grain boundaries were identified by thresholding,

(25) Yu, S. H.; Qian, Y. T.; Shu, L.; Xie, Y.; Yang, L.; Wang, C. S. *Mater. Lett.* **1998**, *35*, 116.
(26) Peng, X. S.; Meng, G. W.; Zhang, J.; Zhao, L. X.; Wang, X. F.; Wang, Y. W.; Zhang, L. D. *J. Phys. D: Appl. Phys.* **2001**, *34*, 3224.
(27) Rincon, M. E.; Sanchez, M.; George, P. J.; Sanchez, A.; Nair, P. K. *J. Solid State Chem.* **1998**, *136*, 167.
(28) Yu, S. H.; Shu, L.; Yang, J.; Zhao, H. H.; Qian, Y. T.; Yu, H. Z. *J. Mater. Res.* **1999**, *14*, 4157.
(29) Nayak, B. B.; Acharya, H. N.; Mitra, G. B.; Mathur, B. K. *Thin Solid Films* **1983**, *105*, 17.
(30) Afzaal, M.; Aucott, S. M.; Crouch, D. J.; O'Brien, P.; Woollins, J. D.; Park, J.-H. *Chem. Vap. Deposition* **2002**, *5*, 186.
(31) Cea-Olivares, R.; Montalvo, V. G.; Novosad, J.; Kilian, P.; Woollins, J. D.; Slawin, A. M. Z.; Garcia, P. G. Y.; Lopez-Cardoso, M.; Espinosa-Perez, G.; Toscano, R. A.; Hernandez, S.; Canseco-Melchor, G.; Lima-Montano, L.; Rodriguez-Narvaez, C. *Phosphorus, Sulfur Silicon Relat. Elem.* **1997**, *125*, 347.
(32) Crouch, D. J.; Helliwell, M.; O'Brien, P.; Park, J.-H.; Waters, J.; Williams, D. J. *Dalton Trans.* **2003**, 1500.
(33) Sheldrick, G. M. *SHELXL 97* and *SHELXS 97*; University of Göttingen: Göttingen, Germany, 1997.
(34) Bruker. *SHELXTL*, Version 6.10; Bruker AXS Inc.: Madison, WI, 2000.
(35) Cousins M. A.; Durose, K. *Thin Solid Films* **2000**, *361−362*, 253.

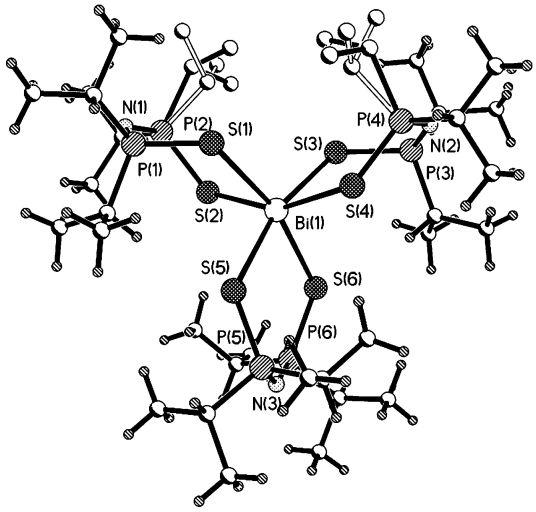

Figure 1. X-ray crystal structure of $Bi[(SP^iPr_2)_2N]_3$.

using matrix refined data from a scanned SEM micrograph. Modified images were skeletonized via iterative reduction of grain boundary widths. Grain sizes were described quantitatively by application of the concept of equivalent radius. Statistical data were obtained using a spreadsheet program.

3. Results and Discussion

The dichalcogenoimidodiphoshanto compounds, $Bi[(EPR_2)_2N]_3$ (E: S, Se; R = Ph, ^{i}Pr) used in this study were found to be ideal for use as single-source precursors; they are air-stable and readily obtained in good synthetic yields. The precursor $Bi[(SeP^iPr_2)_2N]_3$ sublimes at ca. 320−350 °C, leaving ca. 25% residue at atmospheric pressure, while the sulfur-containing analogue, $Bi[(SP^iPr_2)_2N]_3$, sublimes at 230−280 °C, leaving only ca. 10% residue. By contrast, $Bi[(SPPh_2)_2N]_3$ sublimes at higher temperature (370−400 °C), leaving ca. 40% residue and hence this compound proved to be less effective as a precursor for LP-MOCVD. $Bi[(SePPh_2)_2N]_3$ was found to sublime at 350−400 °C and leave a considerable amount of residue (ca. 35%), but despite relatively poor volatility it was used successfully for the deposition of BiSe films by LP-MOCVD.

The residue obtained from pyrolysis of $Bi[(SPPh_2)_2N]_3$ at 600 °C for 1 h was characterized by XRPD. Comparison of the results with data on the JCPDS led to the conclusion that the residue comprised a mixture of BiS_2, Bi_2S_3, bismuth, and phosphorus. EDAX analysis of the residue revealed the presence of bismuth (ca. 16%), sulfur (ca. 25%), and phosphorus (ca. 58%). It is noted that the Bi:S ratio of the precursor residue is very close to that seen in the films produced by AACVD of $Bi[(SPPh_2)_2N]_3$.

The pyrolysis of $Bi[(SeP^iPr_2)_2N]_3$ resulted in a residue which was intractable to XRPD analysis, although there is some indication for the presence of selenium (JCPDS 24-0714) or Bi_2Se_3 (JCPDS 33-0214).

3.1. Single-Crystal X-ray Diffraction Study of $Bi[(SP^iPr_2)_2N]_3$. Crystals of $Bi[(SP^iPr_2)_2N]_3$ were obtained by evaporation of a THF solution at room temperature. The crystal structure of the compound is shown in Figure 1 and crystallographic data and selected bond angles and bond distances are given in Tables 1 and 2, respectively. The crystalline phase of the compound belongs to the monoclinic space group *Cc* and has crystallographic 2-fold symmetry. In the structure, the bismuth atom is coordinated to six sulfur atoms in a distorted octahedral geometry. Williams et al. suggest, in their study on the analogous compound $Bi[(SPPh_2)_2N]_3$,[36] that the Bi − S bonds on one triangular face should be elongated, due to the repulsive effect of the lone pair of electrons on the bismuth atom. This effect seems apparent in the bond lengths of Bi−S1 and 3 bonds (2.831 Å(2)), which are longer than the Bi−S2 and 4 bonds (2.775 Å(2)). In contradiction to this,

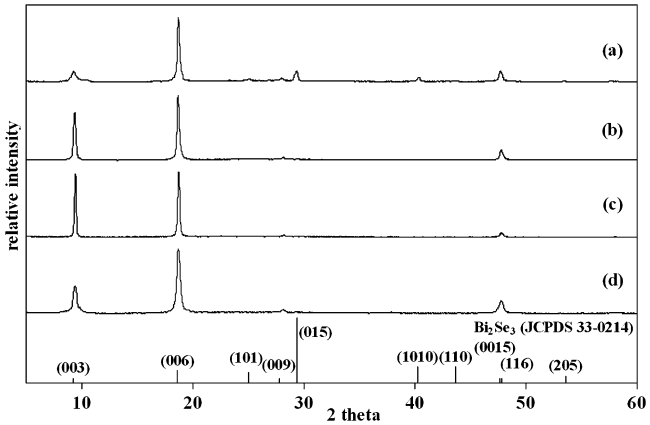

Figure 2. XRPD patterns of films grown by LP-MOCVD of $Bi[(SeP^iPr_2)_2N]_3$ at (a) T_{prec} = 275 °C, T_{subs} = 425 °C, (b) T_{prec} = 225 °C, T_{subs} = 425 °C, (c) T_{prec} = 225 °C, T_{subs} = 400 °C, and (d) T_{prec} = 225 °C, T_{subs} = 375 °C.

Table 3. Details of Bismuth Selenide Growth Experiments

run	deposition technique	precursor	T_{prec} (°C)	argon flow rate (sccm)	T_{subs} (°C)	stoichiometry
1	LP-MOCVD	$Bi[(SeP^iPr_2)_2N]_3$	275	N/A	425	Bi_2Se_3
2	LP-MOCVD	$Bi[(SeP^iPr_2)_2N]_3$	250	N/A	450	Bi_2Se_3
3	LP-MOCVD	$Bi[(SeP^iPr_2)_2N]_3$	250	N/A	425	Bi_2Se_3
4	LP-MOCVD	$Bi[(SeP^iPr_2)_2N]_3$	225	N/A	425	Bi_2Se_3
5	LP-MOCVD	$Bi[(SeP^iPr_2)_2N]_3$	225	N/A	400	Bi_2Se_3
6	LP-MOCVD	$Bi[(SeP^iPr_2)_2N]_3$	225	N/A	375	Bi_2Se_3
7	LP-MOCVD	$Bi[(SePPh_2)_2N]_3$	275	N/A	450	BiSe
8	LP-MOCVD	$Bi[(SePPh_2)_2N]_3$	300	N/A	425	BiSe
9	LP-MOCVD	$Bi[(SePPh_2)_2N]_3$	300	N/A	450	BiSe
10	AACVD	$Bi[(SeP^iPr_2)_2N]_3$	N/A	140	475	Bi_2Se_3

Table 4. Details of Bi_2S_3 Growth Experiments

run	deposition technique	precursor	T_{prec} (°C)	argon flow rate (sccm)	T_{subs} (°C)	stoichiometry
11	LP-MOCVD	$Bi[(SP^iPr_2)_2N]_3$	250		350	Bi_2S_3
12	LP-MOCVD	$Bi[(SP^iPr_2)_2N]_3$	250		375	Bi_2S_3
13	LP-MOCVD	$Bi[(SP^iPr_2)_2N]_3$	250		400	Bi_2S_3
14	LP-MOCVD	$Bi[(SP^iPr_2)_2N]_3$	250		425	Bi_2S_3
15	AACVD	$Bi[(SP^iPr_2)_2N]_3$		140	400	Bi_2S_3
16	AACVD	$Bi[(SP^iPr_2)_2N]_3$		140	425	Bi_2S_3
17	AACVD	$Bi[(SP^iPr_2)_2N]_3$		140	450	Bi_2S_3
18	AACVD	$Bi[(SP^iPr_2)_2N]_3$		140	475	Bi_2S_3
19	AACVD	$Bi[(SP^iPr_2)_2N]_3$		200	400	Bi_2S_3
20	AACVD	$Bi[(SP^iPr_2)_2N]_3$		200	425	Bi_2S_3
21	AACVD	$Bi[(SP^iPr_2)_2N]_3$		200	450	Bi_2S_3
22	AACVD	$Bi[(SP^iPr_2)_2N]_3$		200	475	Bi_2S_3
23	AACVD	$Bi[(SPPh_2)_2N]_3$		200	425	Bi_2S_3
24	AACVD	$Bi[(SPPh_2)_2N]_3$		200	450	Bi_2S_3
25	AACVD	$Bi[(SPPh_2)_2N]_3$		200	475	Bi_2S_3
26	AACVD	$Bi[(SPPh_2)_2N]_3$		140	450	Bi_2S_3
27	AACVD	$Bi[(SPPh_2)_2N]_3$		140	475	Bi_2S_3

(36) Williams, D. J.; Quicksall, C. O.; Barkigia, K. M. *Inorg. Chem.* **1982**, *21*, 2097.

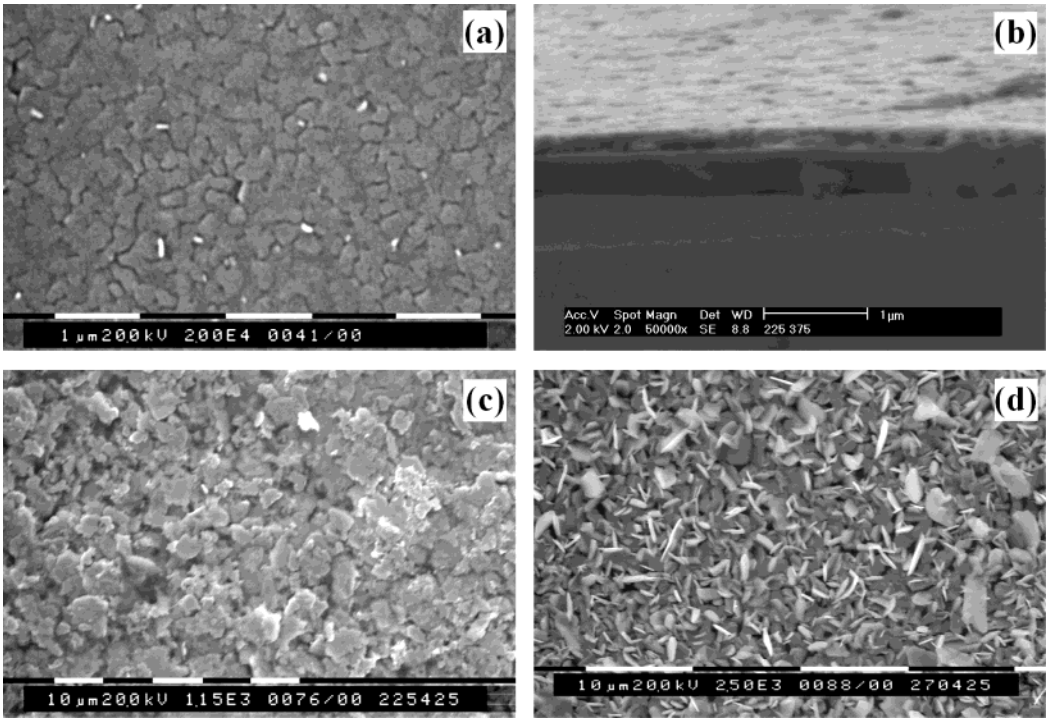

Figure 3. SEM micrographs of films grown by LP-MOCVD of $Bi[(SeP^iPr_2)_2N]_3$ at (a) and (b) T_{prec} = 225 °C, T_{subs} = 375 °C, (c) T_{prec} = 225 °C, T_{subs} = 425 °C, and (d) T_{prec} = 275 °C, T_{subs} = 425 °C.

however, the Bi−S5 and 6 bonds are equal in length (2.843 Å(2)). Inspection of the S−Bi−S bond angles yields no evidence for any structural distortion due to the electron lone pair on bismuth, leading to the conclusion that steric effects override the electronic effects on the structure of this compound. This is also seen to be the case in the selenium analogue, $Bi[(SeP^iPr_2)_2N]_3$,[32] which shows the same pattern of bismuth−chalcogenide bond lengths.

3.2. Bi_2Se_3 via LP-MOCVD of $Bi[(SeP^iPr_2)_2N]_3$. All films deposited on glass substrates by LP-MOCVD were silver/gray and specular. A summary of all successful growth experiments is given in Tables 3 and 4. Films were deposited at substrate temperatures (T_{subs}) of 375−450 °C, with precursor temperatures (T_{prec}) of 225−275 °C. Films grown at higher T_{prec} (275 °C) tended to be slightly powdery, while lower T_{prec} (225−250 °C) gave rise to specular films. It was also noted that at higher growth temperatures (425−450 °C) film growth occurred mainly at the edges of the substrate, whereas lower growth temperatures (375−400 °C) gave more uniform substrate coverage.

The XRPD patterns (Figure 2) indicate the presence of rhombohedral Bi_2Se_3 (JCPDS: 33-214), with texturing evident by the enhanced (006) signal. It was initially suspected, based on the XRPD pattern of the film deposited with T_{prec} = 225 °C, T_{subs} = 400 °C, that a mixture of hexagonal BiSe (JCPDS: 29-246) and rhombohedral Bi_2Se_3 was present. However, EDAX analysis on random sites of the film showed that the Bi:Se ratio was close to 2:3. It was hypothesized that variation of growth temperature led to various phases of thin film material, as was observed by Haggata et al.[37] In their study, films of different phases of indium sulfide, InS, In_6S_7, and β-In_2S_3, were deposited from mixed alkyl dithiocarbamato indium precursors of general formula $R_2MS_2CNEt_2$, where R = Me, Et, or neopentyl. However, our continued investigation suggests that this is not the case since subsequent repetitions of the growth experiment at T_{prec} = 225 °C, T_{subs} = 400 °C resulted in single-phase Bi_2Se_3.

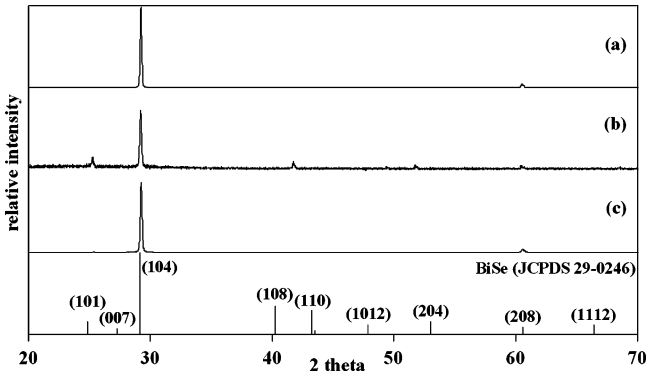

Figure 4. XRPD patterns of films grown via LP-MOCVD of $Bi[(SePPh_2)_2N]_3$ at (a) T_{prec} = 300 °C, T_{subs} = 450 °C, (b) T_{prec} = 300 °C, T_{subs} = 425 °C, and (c) T_{prec} = 275 °C, T_{subs} = 450 °C.

It is apparent from the XRPD patterns that the intensity of the (003) reflection varies widely. The intensity shows some correlation with the percentage of Se as indicated by EDAX. The films deposited at T_{prec} = 225, T_{subs} = 400 or 425 °C contain ca. 61.5% selenium and have (003) peaks of similar intensity. The film deposited at T_{prec} = 275 °C, T_{subs} = 425 °C contains slightly less selenium (60%) and a (003) peak of much lower intensity, compared to the (006) plane which has 100% relative intensity. However, this correlation is unlikely to be causal, especially as the percentage error inherent in the EDAX technique employed means that the variation in selenium content is of little experimental significance.

(37) Haggata, S. W.; Malik, M. A.; Motevalli, M.; O'Brien, P. *Chem. Mater.* **1995**, *7*, 716.

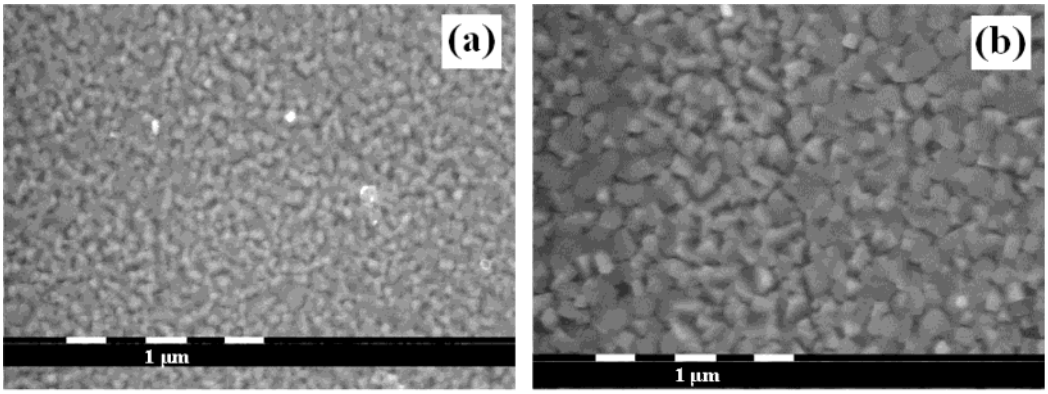

Figure 5. SEM micrographs of films grown via LP-MOCVD of $Bi[(SePPh_2)_2N]_3$at (a) T_{subs} = 425 °C and (b) T_{subs} = 450 °C, with T_{prec}= 300 °C.

SEM images reveal that the films consist of densely packed grains (Figure 3). At higher growth temperatures (425−450 °C), an increase in particle size was observed. For example, grains of up to 10 μm in diameter were seen in the film deposited at T_{subs} = 425 °C (Figure 3c) compared with grains of ca. 200-nm diameter at lower growth temperature (375 °C) (Figure 3a). The film deposited at T_{prec} = 275 °C, T_{subs} = 425 °C (Figure 3d) is seen to differ from the others in that it consists of randomly oriented platelets ca. 2 μm in diameter. In each case, the elemental ratio obtained by EDAX is in agreement with the structure indicated by XRPD, with Bi:Se ratios of ca. 2:3, although in general the films are slightly selenium-rich. The thickness of the film deposited at T_{subs} = 375 °C can be estimated from the SEM micrograph to be ca. 100 nm (growth rate: ca. 100 nm/h).

3.3. BiSe via LP-MOCVD of $Bi[(SePPh_2)_2N]_3$. Films were deposited on glass substrates from $Bi[(SePPh_2)_2N]_3$ at T_{subs} = 425−450 °C, T_{prec} = 275−300 °C. The films deposited at T_{subs} = 450 °C were specular and silver-colored, while the film deposited at T_{subs} = 425 °C was powdery and blue/gray in color. The XRPD patterns indicate that the films comprise of hexagonal BiSe with a preferred orientation in the (104) plane (Figure 4). Study by SEM reveals the films to be granular in composition, with higher growth temperature resulting in larger grains (Figure 5). At T_{subs} = 450 °C the grains are seen to be ca. 400−700 nm, whereas the grains in the films deposited at T_{subs} = 425 °C appear to be much smaller (ca. 100−300 nm). The thickness of the film deposited at T_{subs} = 375 °C can be estimated from the SEM micrograph to be ca. 100 nm, implying a growth rate of ca. 100 nm/h.

It is important to note that the *iso*propyl and phenyl substituted precursors lead exclusively to monophasic Bi_2Se_3 and BiSe, respectively. The reasoning for this phenomenon is highly speculative, but it seems likely that the difference in electron-donating character of the alkyl groups on the P atoms affects the relative bond strengths within the structures and hence the decomposition profiles of the parent molecules. This could potentially have a significant impact on the relative amounts of bismuth and selenium reaching, or being retained, at the substrate surface.

3.4. Bi_2Se_3 by AACVD of $Bi[(SeP^iPr_2)_2N]_3$. Films were deposited via AACVD of $Bi[(SeP^iPr_2)_2N]_3$ at T_{subs} = 475 °C, with constant carrier gas flow rate of 140 sccm. No significant deposition, in terms of film thickness or crystallinity, was noted at higher or lower growth temperatures. The XRPD pattern (Figure 6) indicates that the deposited material is Bi_2Se_3, with a preferred orientation along the (006) direction. The XRPD pattern for the film deposited by AACVD of $Bi[(SeP^iPr_2)_2N]_3$ showed much higher peak intensities than the films deposited by LP-MOCVD, indicating that the film deposited by AACVD was of improved crystallinity. EDAX analysis indicates the film to be slightly selenium-deficient, with a selenium content of ca. 57%. The film was shown by SEM to comprise polygonal grains in a dense basal layer (Figure 7).

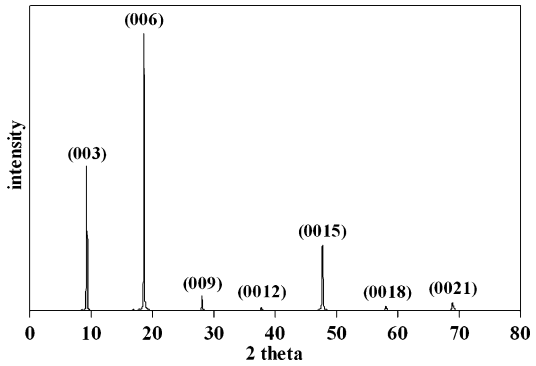

Figure 6. XRPD pattern of Bi_2Se_3 deposited from $Bi[(SeP^iPr_2)_2N]_3$ by AACVD at T_{subs} = 475 °C, with an argon flow rate of 140 sccm.

Grain size studies (see Experimental Section) have been performed on the film grown from $Bi[(SeP^iPr_2)_2N]_3$ by AACVD at T_{subs} = 475 °C with an argon carrier gas flow rate of 140 sccm. In typical thin film growth, the grain size distribution tends not to be "normal" but rather to be skewed toward larger particles, as a result of processes that drive toward minimization of surface energy. The results of this analysis show the grain sizes to broadly follow a normal Gaussian distribution. However, there was a distinct periodicity in the development of grain size; that is, at defined intervals (~300 nm) the grain size distribution deviated, in that it was greater than expected for a normal distribution (Figure 8). This may be indicative of an increased stability associated with grains of these sizes, or stepwise grain growth by 0.3-μm increments.

3.5. Bi_2S_3 via LP-MOCVD of $Bi[(SP^iPr_2)_2N]_3$. Deposition experiments were carried out using $Bi[(SP^iPr_2)_2N]_3$ at growth temperatures of 350−425 °C,

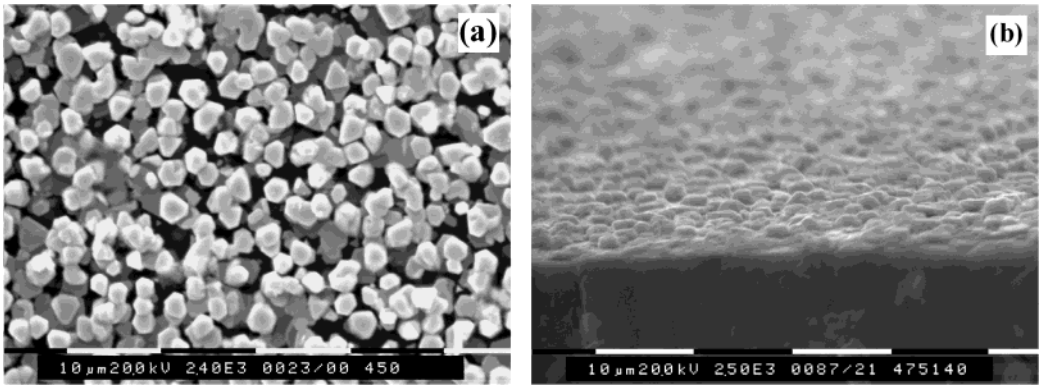

Figure 7. SEM micrographs of Bi_2Se_3 deposited from $Bi[(SeP^iPr_2)_2N]_3$ by AACVD at T_{subs} = 475 °C, with an argon flow rate of 140 sccm.

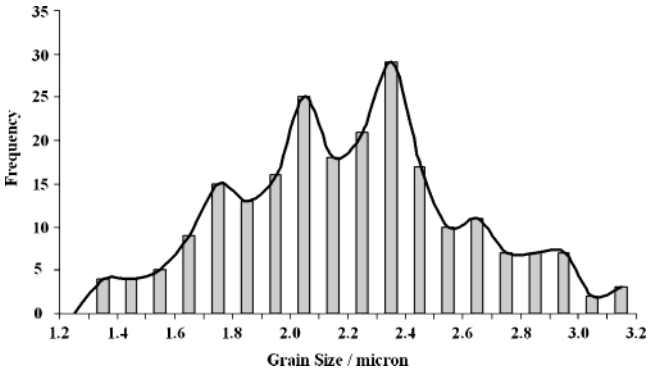

Figure 8. Graph of size distribution of grains in the film deposited by AACVD of $Bi[(SeP^iPr_2)_2N]_3$ by AACVD at T_{subs} = 475 °C, with an argon flow rate of 140 sccm.

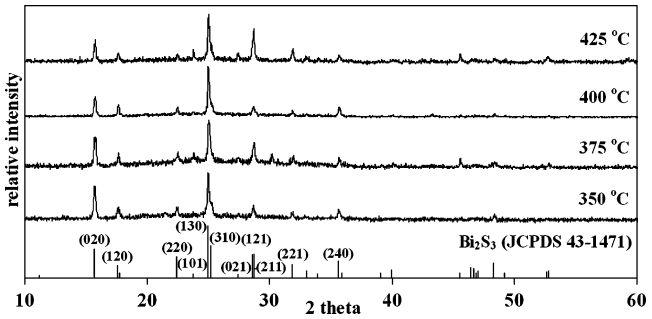

Figure 9. XRPD patterns of films grown via LP-MOCVD of $Bi[(SP^iPr_2)_2N]_3$ with T_{subs} = 250 °C. Temperatures indicate growth temperature.

with precursor temperatures of 250 and 275 °C. XRPD analysis indicates that the deposited material is orthorhombic Bi_2S_3 with a preferred orientation in the (130) direction (Figure 9). Quantitative EDAX analysis confirms that in all cases the elemental composition is close to 2:3, in good agreement with the stoichiometry indicated by XRPD analysis. SEM studies show that the films deposited at T_{prec} = 250 °C comprise granules of Bi_2S_3 ca. 0.1−0.4 μm in diameter (Figure 10a,b), while those films deposited at T_{prec} = 275 °C were mixtures of rods and irregular platelets. From inspection of cross-sectional SEM micrographs of the films deposited with T_{prec} = 250 °C, the film thickness, and hence the growth rate per hour, can be estimated. The growth rates for the films deposited at T_{subs} = 350, 375, 400, and 425 °C are ca. 0.24, 0.42, 0.54, and 0.58 μm/h, respectively. In this case, higher substrate temperature clearly leads to higher growth rates, with this effect markedly reduced above 400 °C.

The kinetics of bismuth sulfide grain growth was investigated via analysis of grain size distributions, as described earlier, on films deposited at T_{prec} = 250 °C, T_{subs} = 375 °C, after 15, 30, 45, and 60 min of growth (Figure 11). Mean grain size was plotted as a function of time (Figure 12), revealing that grain growth accelerates from the onset of deposition, to a peak at between 30 and 45 min, before leveling off after 45 min, possibly due to the exhaustion of the precursor.

It is evident from Figure 11a that, in films grown for 15 min, there are a significant number of grains that are far larger than the majority of much smaller grains. The observation was initially taken to be an indication of the occurrence of abnormal grain growth.[38,39] However, if this were the case, we would expect to see a pronounced bimodality in the grain distribution after 30 min or more, which is not evident in this study. Grains of diameter approaching ~380 nm are observed after 15 min of growth, while no grains larger than 230 nm are observed after 30 min. This could possibly be explained as an artifact of the analysis program; that is, the boundary between certain grains may not been identified, leading to the identification of artificially large grains in the film grown for 15 min. However, this is unlikely, as numerous large grains are evident in the SEM micrograph of the film grown for 15 min. It would therefore appear that the large grains apparent after 15 min of growth fragment during the subsequent 15 min of growth, or are simply overgrown by subsequent layers of grains, since they are not noted after a growth period of 30 min or more. The incidence of these enlarged grains can be rationalized in terms of undesirable pre-reaction during delivery. This may be a function of either precursor chemistry or reactor geometry. The TGA curve of $Bi[(S^iPrR_2)_2N]_3$ does not show a defined and sharp decomposition temperature; hence, the former may apply. However, no attempts were made to optimize the delivery system. Work to address this issue is in progress.

3.6. Bi_2S_3 by AACVD of $Bi[(SPR_2)_2N]_3$ (R = ^{i}Pr or Ph). Gray films have been deposited from $Bi[(SPR_2)_2N]_3$ (R = ^{i}Pr or Ph) at growth temperatures of 425−475 °C with argon carrier-gas flow rates of 140 and 200 sccm. Very thin films were also deposited at T_{subs} = 400 °C,

(38) Greiser, J.; Müllner, P.; Arzt, E. *Acta Mater.* **2001**, *49*, 1041.
(39) Cocks, A. C. F.; Gill, S. P. A. *Acta Mater.* **1996**, *44*, 4765.

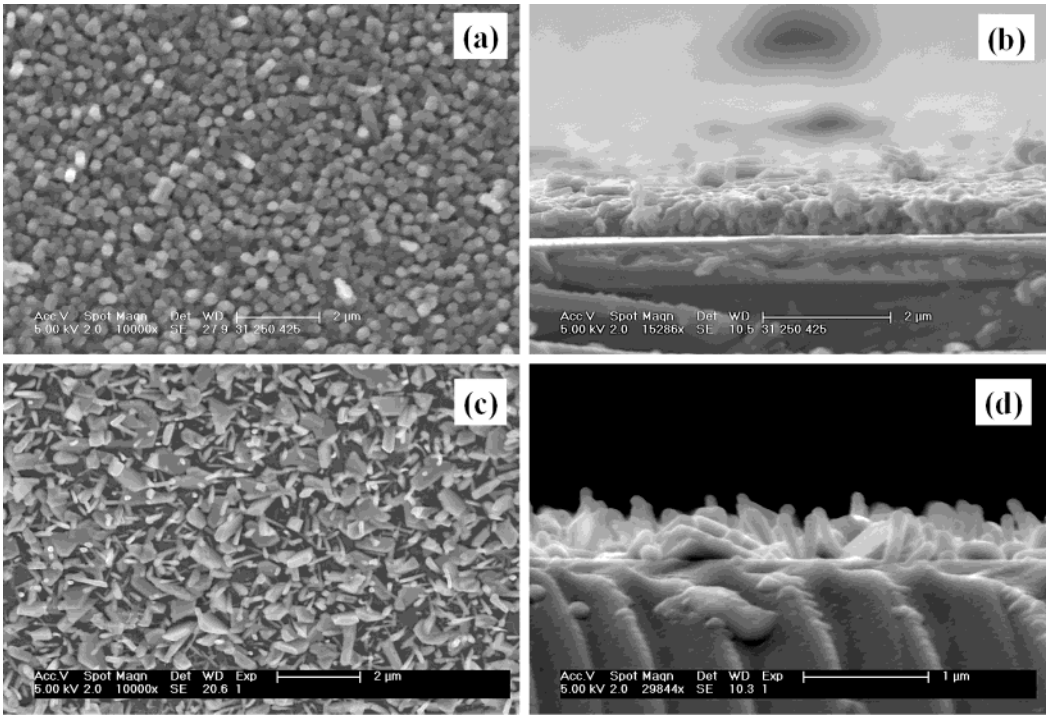

Figure 10. SEM images of films deposited by LP-MOCVD at (a) and (b) $T_{prec} = 250$ °C, $T_{subs} = 425$ °C and (c) and (d) $T_{prec} = 275$ °C, $T_{subs} = 400$ °C.

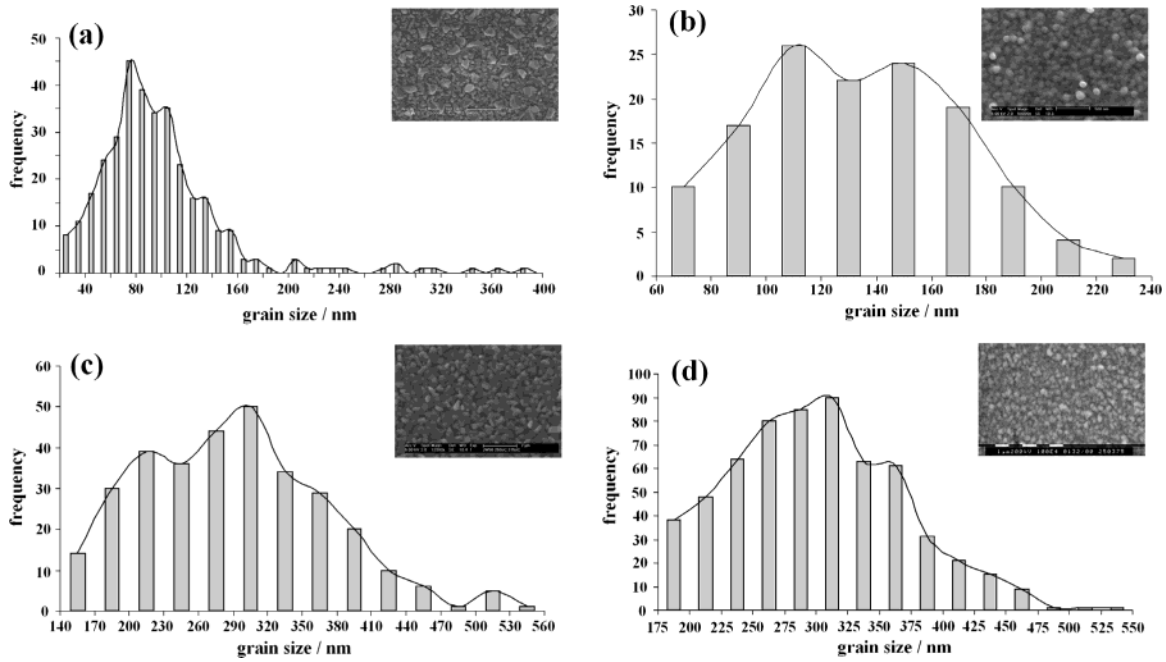

Figure 11. Graphs of grain size distribution in Bi_2S_3 films deposited at $T_{prec} = 250$ °C, $T_{subs} = 375$ °C for (a) 15 min, (b) 30 min, (c) 45 min, and (d) 60 min.

and although subsequent analysis showed these to be of poor morphology and crystallinity, they were sufficiently transparent to permit band gap determination via electronic spectroscopy. The band gaps of these films were found to be ca. 1.32 eV, in good agreement with the literature value of 1.3 eV for the direct band gap of Bi_2S_3.[14]

3.6.1. Bi_2S_3 by AACVD of $Bi[(SP^iPr_2)_2N]_3$. The films have been confirmed by XRPD to be composed of orthorhombic Bi_2S_3 with preferred orientation in either the (130), (310), or (211) direction (Figure 13), dependent on the growth parameters. However, low peak intensities indicate that the material is of low crystallinity. EDAX analyses show that the films are bismuth-rich, containing ca. 45−50% bismuth. It is observed that the films deposited with carrier gas flow rates of 200 sccm contain ca. 2−3% more sulfur than the films deposited with the same growth temperature at 140 sccm. It is also observed that the films deposited at 450 °C contain 2−3% more sulfur than films deposited at 425 or 475 °C.

SEM studies show distinctly different morphology under each set of growth conditions. Deposition at 425 °C, with a flow rate of 140 sccm, leads to the formation of rods of ca. 100-nm thickness, whereas a flow rate of

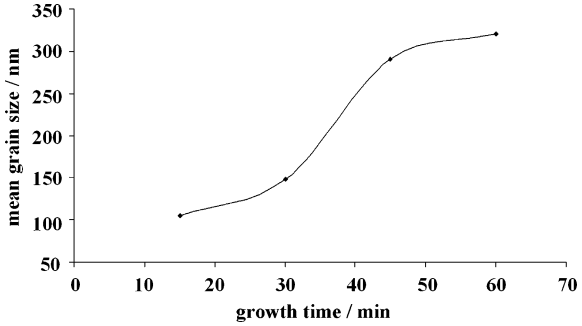

Figure 12. Graph of mean grain size in Bi_2S_3 films deposited at T_{prec} = 250 °C, T_{subs} = 375 °C.

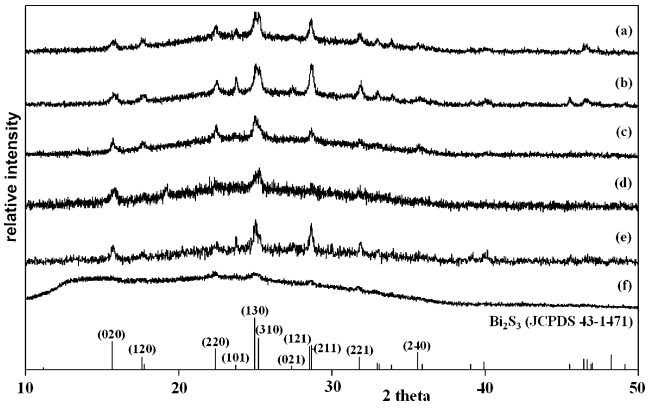

Figure 13. XRPD patterns of films deposited via AACVD of $Bi[(SP^iPr_2)_2N]_3$ at (a) T_{subs} = 475 °C, flow rate = 200 sccm, (b) T_{subs} = 450 °C, flow rate = 200 sccm, (c) T_{subs} = 425 °C, flow rate = 200 sccm, (d) T_{subs} = 475 °C, flow rate = 140 sccm, (e) T_{subs} = 450 °C, flow rate = 140 sccm, and (f) T_{subs} = 425 °C, flow rate = 140 sccm.

200 sccm gives rise to rectangular platelets of up to 4 μm in length. Growth at 450 °C, with a flow rate of 140 sccm, results in the deposition of irregular agglomerations of rods and platelets. When the argon flow rate is increased to 200 sccm, the deposited film is seen to comprise randomly oriented rods, ca. 500 nm in diameter. Growth at 475 °C resulted in a low-density distribution of platelike granular agglomerations, with a flow rate of 140 sccm, while 200 sccm resulted in a dense layer of platelets of up to ca. 3-μm diameter (Figure 14).

3.6.2. Bi_2S_3 by AACVD of $Bi[(SPPh_2)_2N]_3$. XRPD studies show (Figure 15) the films to be composed of orthorhombic Bi_2S_3, with a marked variation in preferred orientation correlating to variations in growth conditions (e.g., growth temperature and argon flow rate). All films show considerable texturing. The film grown at T_{subs} = 425 °C, with an argon flow rate of 200 sccm, has a preferred orientation along the (110) direction, while the film produced at the same argon flow rate, with T_{subs} = 450 °C, has a preferred orientation along the (310) direction. The XRPD pattern of the film deposited at higher growth temperature (475 °C) showed a high degree of orientation along the (220) direction, with the other peaks at much lower relative intensities than those observed in the films grown at lower temperature. The XRPD patterns of the two films deposited with argon flow rates of 140 sccm show that the film deposited at 450 °C has a preferred orientation along the (310) direction while the film grown at 475 °C has a preferred orientation along the (110) direction.

EDAX analysis confirms that the deposited films are Bi-rich and also confirms the presence of trace amounts of phosphorus (≤3%). On comparison of EDAX and XRPD data, it is noted that the film grown at 475 °C with a carrier gas flow rate of 200 sccm, which is the only film showing an elemental ratio close to that

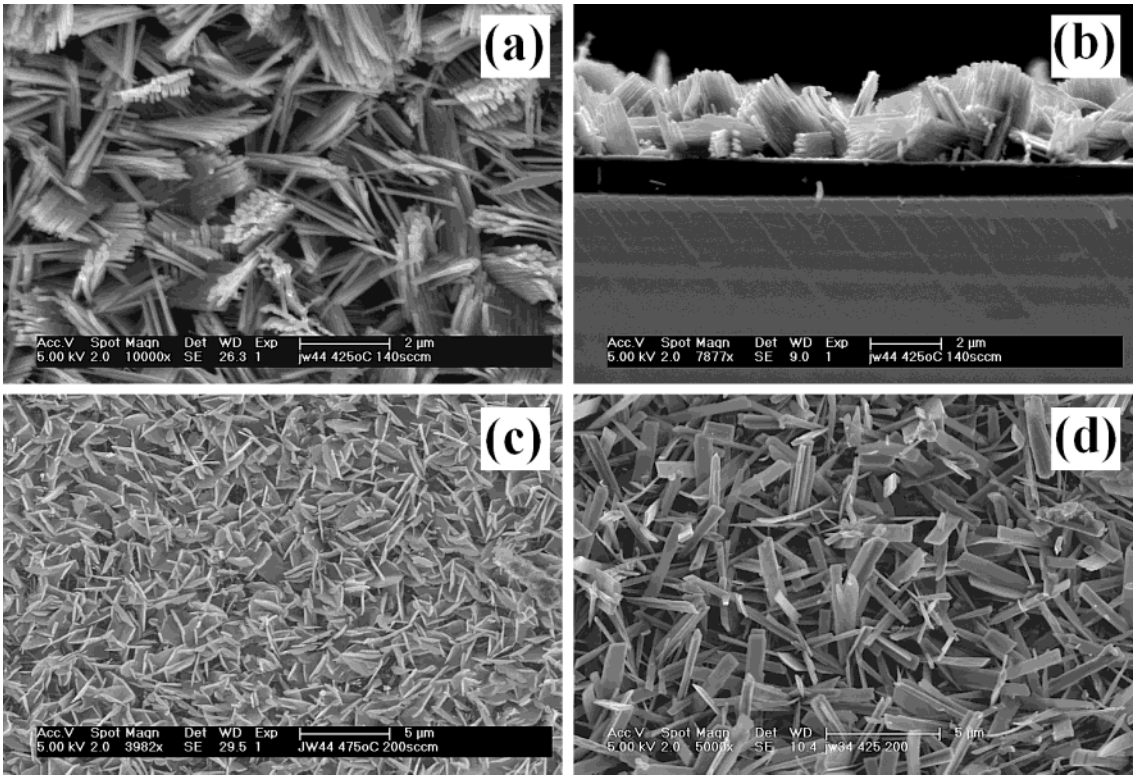

Figure 14. SEM micrographs of Bi_2S_3 films grown via AACVD of $Bi[(SP^iPr_2)_2N]_3$ at (a) and (b) T_{subs} = 475 °C, flow rate = 140 sccm, (c) T_{subs} = 475 °C, flow rate = 200 sccm, and (d) T_{subs} = 425 °C, flow rate = 200 sccm.

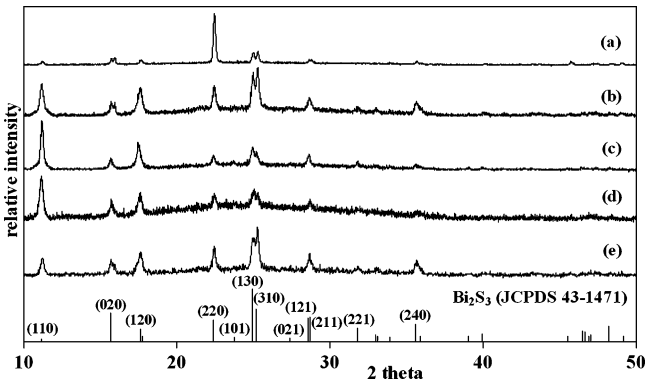

Figure 15. XRPD patterns of films deposited via AACVD of $Bi[(SPPh_2)_2N]_3$ at (a) T_{subs} = 475 °C, flow rate = 200 sccm, (b) T_{subs} = 450 °C, flow rate = 200 sccm, (c) T_{subs} = 425 °C, flow rate = 200 sccm, (d) T_{subs} = 475 °C, flow rate = 140 sccm, and (e) T_{subs} = 450 °C, flow rate = 140 sccm.

predicted by XRPD (43% Bi, 57% S), shows a high degree of orientation, with the (220) peak being ca. 4 times the intensity of the second most intense peak (Figure 11c). However, the other films deposited from $Bi[(SPPh_2)_2N]_3$ via AACVD contain ≥48% bismuth and show much lower degrees of orientation, with the 100% peaks in their XRPD patterns being no more than twice the intensity of the second most intense peak. Furthermore, it is observed that the peak relating to the (110) plane is absent or of low relative intensity in films with elemental ratios close to 2:3, including the film deposited at 475 °C with a carrier gas flow rate of 200 sccm and in those films deposited via LP-MOCVD of $Bi[(SP^iPr_2)_2N]_3$. Conversely, the (110) peak is among the most intense peaks in the bismuth-rich films deposited via AACVD of $Bi[(SPPh_2)_2N]_3$. This suggests that the intensity of the (110) peak is related to the amount of bismuth in the material since the peak is present in those films, which are heavily bismuth-rich while being absent, or of very low intensity, in those films having elemental ratios of close to 2:3 (Bi:S). It is therefore interesting to observe that the (110) peak is also absent from those films deposited via AACVD of $Bi[(SP^iPr_2)_2N]_3$, despite these films containing similar proportions of bismuth to those deposited via AACVD of $Bi[(SPPh_2)_2N]_3$.

SEM studies reveal that the films deposited with a carrier gas flow rate of 140 sccm consist of a mixture of platelets and fibers, with a base layer of granular material visible where the overlying material is least dense. Deposition at 425 and 450 °C, with a carrier gas flow rate of 200 sccm, yielded rectangular platelets. Higher growth temperatures appear to promote the growth of rodlike structures since the platelets deposited at 450 °C were narrower and more rodlike than those grown at 425 °C. The trend is continued at 475 °C, with the deposition of a sparse layer of fibrous agglomerations on a base layer of grains.

The base layer of grains evident in each of the films grown from $Bi[(SPPh_2)_2N]_3$ indicates two distinct growth steps, as no fibers are discernible within the grain layer, suggesting that initial deposition was in the form of grains, followed by the formation of fibers. However, grains are clearly discernible on some of the larger features in the film deposited at T_{subs} = 475 °C, with a flow rate of 200 sccm, indicating continuous grain growth. It is therefore possible that the rods or platelets are the products of pre-reactions and are formed en route to the substrates. EDAX analysis was performed on both the fibers and the underlying grain layer and showed that both morphological formations had similar elemental compositions, with ca. 65% bismuth.

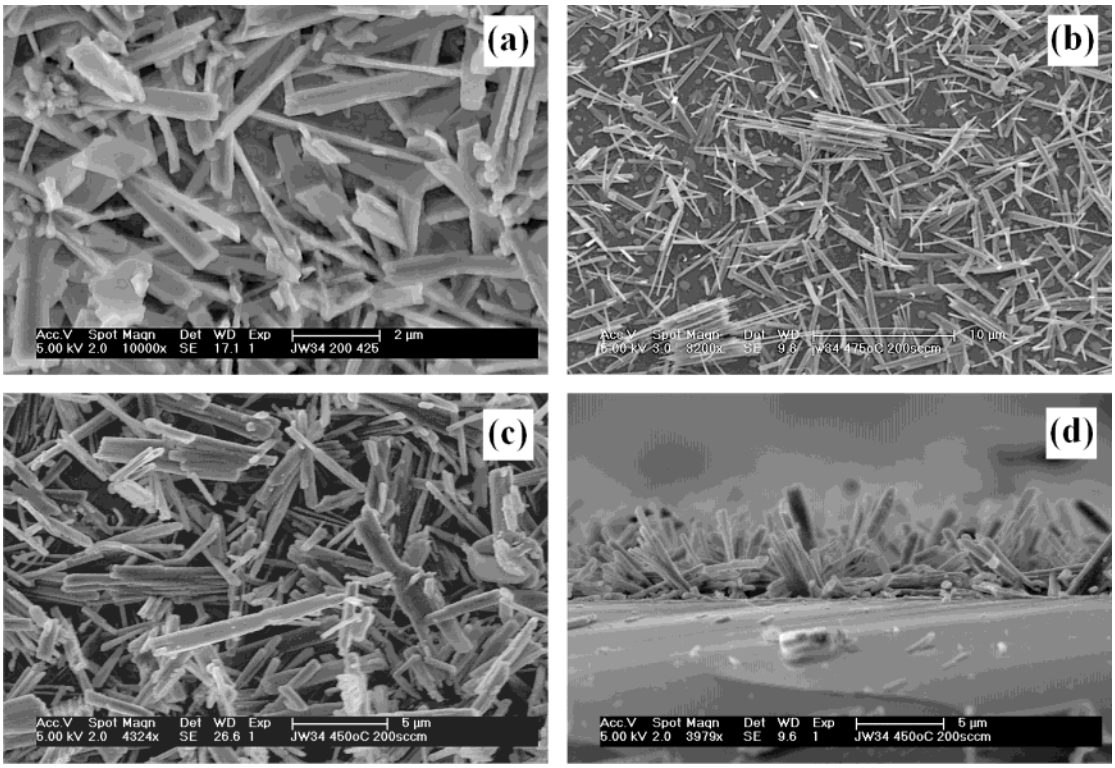

Figure 16. SEM micrographs of Bi_2S_3 films grown via AACVD of $Bi[(SPPh_2)_2N]_3$ at (a) T_{subs} = 425 °C, flow rate = 200 sccm, (b) T_{subs} = 475 °C, flow rate = 200 sccm, and (c) and (d) T_{subs} = 450 °C, flow rate = 200 sccm.

It is noted that none of the Bi_2S_3 films in this study show similar morphology to those deposited from $Bi(S_2CNMeHex)_3$ by LP-MOCVD,[22] although some resemblance is observed to the rod- or fiber-like structures in a number of the films in this study (Figures 10, 14, and 16).

4. Conclusions

Bismuth chalcogenide thin films have been grown successfully from $Bi[(EPR_2)_2N]_3$ (E = S, Se; R = Ph, ^{i}Pr) precursors by LP and AACVD. By selection of growth technique and precursor it is possible to control the phase and morphology of the deposited material. In this study, deposition of films of rhombohedral Bi_2Se_3, hexagonal BiSe, and orthorhombic Bi_2S_3 has been demonstrated. Deposition of stoichiometric Bi_2Se_3 and BiSe, with no phosphorus contamination, has been confirmed by XRPD and EDAX. It was found that LP-MOCVD yields films of higher quality than those deposited by AACVD since the Bi_2S_3 films deposited via LP-MOCVD exhibited no detectable phosphorus contamination and had elemental compositions in good agreement with the stoichiometry indicated by XRPD.

Acknowledgment. The authors are grateful to the EPSRC for financial support.

CM035287O